Agricultural and Forest Meteorology 331 (2023) 109351

Contents lists available at ScienceDirect

Agricultural and Forest Meteorology

journal homepage: www.elsevier.com/locate/agrformet

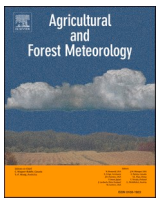

Viticulture adaptation to global warming: Modelling gas exchange, water status and leaf temperature to probe for practices manipulating water supply, canopy reflectance and radiation load

O. Garcia-Tejera [a,*], M. Bonada [b], P.R. Petrie [b,c], H. Nieto [d], J. Bellvert [e], V.O. Sadras [b]

[a] Departamento de Ingeniería Agraria y del Medio Natural, Universidad de La Laguna, Ctra. Geneto, 2, La Laguna, Tenerife 38200, Spain
[b] The South Australia Research and Development Institute, and the School of Agriculture, Food and Wine, The University of Adelaide, Waite Campus, Urrbrae, Australia
[c] The University of New South Wales, Australia and Flinders University, Kensington, Sydney, Bedford Park, Adelaide, NSW 2052, Australia
[d] Institute of Agricultural Sciences, ICA-CSIC, Madrid 28006, Spain
[e] Efficient Use of Water Program, Institut de Recerca i Tecnologia Agroalimentàries (IRTA), Parc de Gardeny, Edifici Fruitcentre, Lleida 25003, Spain

ARTICLE INFO

Keywords:
Modelling
Canopy temperature
Heatwave
Grapevine
Vapour pressure deficit
Radiation

ABSTRACT

Associated with climate change, the frequency, duration, and intensity of heatwaves are increasing in most of the key wine regions worldwide. Depending on timing, intensity, and duration, heatwaves can impact grapevine yield and berry composition, with implications for wine quality. To overcome these negative effects, two types of mitigation practices have been proposed (i) to enhance transpiration and (ii) to reduce the radiation load on the canopy. Here we use a biophysical model to quantify the impact of these practices on canopy gas exchange, vine water status, and leaf temperature (T_l). Model validation was performed in a commercial vineyard. Modelled T_l from 14 to 43 °C, and transpiration, from 0.1 to 5.4 mm d^{-1}, aligned around the identity line with measurements in field-grown vines; the RMSD was 2.6 ºC for temperature and 0.96 mm day^{-1} for transpiration. Trellis system and row orientation modulate T_l. A sprawling single wire trellis with an EW orientation maintained the canopy around 1ºC cooler than a Vertical Shoot Positioned canopy with NS for the same range of total fraction of soil available water (TFAW). Although irrigation before a heatwave is a recommended practice, maximum transpiration can be sustained even when TFAW is reduced, limiting the heat dampening effect of irrigation. Alternatively, canopy cooling can be achieved through Kaolin application, the installation of shade cloth placement, or canopy trimming. Shade cloth produced a greater cooling than Kaolin in all the simulated scenarios; however, T_l differences between them varied. Trimming reduced T_l from 2 ºC to almost 8 ºC compared to its non-trimmed counterpart. Our analysis presents new insights to design heat wave mitigation strategies and supports agronomically meaningful definitions of heat waves that include not only temperature, but also wind, VPD, and radiation load as these factors influence crop physiology under heat stress.

1. Introduction

A heatwave is a succession of days with anomalously high air temperature, with definitions that vary in both temperature thresholds and duration depending on jurisdiction and application (AEMET, 2018; Nairn and Fawcett, 2013). The definitions are based solely on air temperature and do not include other climate factors with agronomical implications, such us wind speed, vapor pressure deficit (VPD) or radiation load.

Worldwide, the frequency, intensity, and duration of heatwaves have increased over the last decades and are projected to increase further (IPCC, 2014, 2018; NOAA, 2020). Heatwaves are known to jeopardize grapevine yield and fruit traits with implications for wine composition and industry sustainability (Webb et al., 2010). Actual damage varies with the timing, intensity, and duration of the heatwave. Bud temperature over 30 °C for two weeks before budburst reduced the number of flowers by up to 18% compared to the control bunches at ambient temperature in Chardonnay (Petrie and Clingeleffer, 2005). Temperature above 35 °C around flowering compromised fruit set and reduced yield the same year (Pagay and Collins, 2017). Elevated temperature 1–2 weeks after veraison compromised the balance between sugars and anthocyanins in berries of Shiraz (Moran et al., 2017; Sadras and Moran,

* Corresponding author.
E-mail address: ogarciat@ull.edu.es (O. Garcia-Tejera).

https://doi.org/10.1016/j.agrformet.2023.109351
Received 5 May 2022; Received in revised form 26 January 2023; Accepted 27 January 2023
Available online 31 January 2023

2012). Later in the season, heat waves can delay ripening and reduce berry size (Greer and Weedon, 2013). Heatwaves during ripening may reduce yield and fruit quality (Webb et al., 2010); excessive solar radiation load leads to physical damage in the bunch (sunburn) and modulates the synthesis and accumulation of the primary and secondary metabolites in the berry (Gambetta et al., 2021). Some traits like berry color, bunch compactness, or canopy growth habit make fruit more vulnerable to extreme temperatures; dark-skin berries exposed to direct sun and low wind, for example, can be up to 15 °C warmer than air temperature (Smart and Sinclair, 1976).

Weather, soil properties (e.g., water holding capacity), and crop water status during a heatwave modulate heat damage (Webb et al., 2010). Canopy temperature is the result of the interaction between environmental, management, genetic and physiological variables (Campbell and Norman, 1998; Jackson et al., 1981). Leaf size, leaf area density, and leaf angle distribution influence the radiation absorbed by the canopy (R_{int}) (Campbell and Norman, 1998), which together with air temperature, relative humidity, wind velocity, and canopy and boundary layer conductance determine canopy temperature (Jackson et al., 1981).

Reductions of stomatal conductance (g_s) due to dry soil or high VPD increase canopy temperature; however, the magnitude of such increase is mediated by the boundary layer conductance that underly the degree of coupling of canopy and surrounding air (Campbell and Norman, 1998; Fereres et al., 2014; Jackson et al., 1981; Monteith and Unsworth, 2013). Other factors such as wind speed and vapor concentration affect the resistance of water movement out of the leaf and limit the cooling effect of transpiration (E_p). For example, when wind speed is low and the boundary layer is still, the high concentration of vapor in the vicinity of the stomatal cavity resists E_p and increases canopy temperature. Furthermore, higher stomatal conductance associated with higher leaf temperature enhances canopy cooling capacity when plant water uptake is not constrained (Kostaki et al., 2020; Sadras et al., 2012).

For new vineyards, row orientation and selection of variety can contribute to manage risk of heat waves. For established vineyards, where row orientation and variety are given, heat stress can be managed with practices aimed at either reducing the likelihood of heatwaves at critical periods (e.g., late pruning that shifts critical stages to cooler part of the season (Moran et al., 2017)) or reducing heat damage. Practices to reduce damage, the focus of this paper, included supplementary irrigation to promote evaporative cooling (Hayman et al., 2012; Webb et al., 2010), and reducing canopy radiation load with reflective sprays such as kaolin (Coniberti et al., 2013; Frioni et al., 2019) or shade-cloth (Caravia et al., 2016; Greer and Weedon, 2013). Infrastructure and water availability often limit the use of irrigation to manage heat stress (Sadras and Schultz, 2013). In Australia, for example, supplementary irrigation before a heat wave is widely recommended to enhance plant E_p and favor evaporative cooling. However, water availability from centralized delivery systems or pump capacity on site limit water supply to large vineyards. Similarly, water allocation may be limited during dry years or at the end of the growing season, when heat waves are more likely, reducing the viability of these practices. The efficiency of other practices such as micro-sprinklers within the canopy or overhead irrigation offer a short period of cooling, are constrained by irrigation infrastructure, water availability and quality, and potential for disease development (Caravia et al., 2017).

The effectiveness of practices against heatwaves depends on interacting weather, soil, genotypic, and management factors. Supplementary irrigation before a heatwave that favors evaporative cooling is likely to be more effective in a dry environment, such as the Barossa Valley in South Australia, than in the more humid Hunter Valley in eastern Australia. In the continuum from anisohydric to isohydric phenotypes, irrigation is more likely to effectively reduce canopy temperature in Shiraz than in Grenache (Schultz, 2003). Shading involves a trade-off with reduced photosynthesis that may affect yield and fruit composition (Greer and Weedon, 2013). These multiple interactions underpin the effectiveness of practices against heat waves and need to be considered when tailoring solutions to complex problems. Models are a scientifically robust, cost-effective approach to quantify the multiple interactions between soil, plant, management, and weather, that are intractable experimentally (Knowling et al., 2021). In this paper we use a biophysical model accounting for vine, soil, management, and weather. The model combines the catenary hypothesis (van den Honert, 1948) with the energy balance at the leaf to explore the responses of three key plant traits – leaf temperature, canopy transpiration, and stem water potential – in response to irrigation interacting with managing practices to modify canopy radiation load by (1) shifting row orientation, (2) increasing canopy reflectance with kaolin, (3) reducing intercepted radiation with shade-cloth, and (4) canopy trimming. Whereas first principles predict a smaller difference in temperature between canopy and air with higher wind speed and smaller leaves, here we quantify these relationships to inform practices.

2. . Materials and methods

2.1. SPAC—CN model

We advance a *SPAC—CN* model combining the soil-plant-atmosphere continuum (SPAC) developed by Garcia-Tejera et al. (2017a) with a canopy temperature module as proposed in Campbell and Norman (1998). Briefly, the SPAC model simulates canopy transpiration (E_p, mm day^{-1}) and stem water potential (Ψ_{stem}, kPa) using the catenary hypothesis (van den Honert, 1948), in which the soil-plant-atmosphere system is viewed as a set of resistances either in parallel or in series. The canopy is discretized into sun/shade leaves (dePury and Farquhar, 1997). The soil is divided vertically into n layers, and horizontally into two compartments; the wet compartment (F_{wet}), which includes the area influenced by the emitters, and the dry compartment (F_{dry}), which represents the rest of the soil. Stomatal conductance (g_s, mol m^{-2} s^{-1}) is simulated using the model of Tuzet et al. (2003), which includes the effect of water potential on stomatal conductance. Radiation interception and absorption are calculated with the approach by Parry et al. (2019) for grapevines, assuming a rectangular canopy.

The model works on a sub-daily time-step and assumes: (1) no leaf or root damage due to extreme temperature (Bita and Gerats, 2013; Wahid et al., 2007); (2) no trunk or leaves water capacitance included in E_p calculations (Jones, 2013), and (3) no changes on intercepted radiation by leaf angle modification due to wilting (Harris et al., 1988).

Our model captures the interaction between plant, soil and weather elements modulating leaf temperature during a heat wave but does not account for plant physiological processes defining plant acclimation and recovery in response to sublethal temperatures (Carvalho et al., 2015; Liu et al., 2014). Similarly, the model lacks temperature thresholds that may trigger permanent leaf damage in response heat stress. These limitations bound our conclusions to heat ways of short duration, and avoid us to explore, for example, the potential damage cause by heatwaves of longer duration or due to repeated heatwaves during the season.

For each leaf class (sunlit or shade), leaf temperature (T_l, °C) is computed as (Campbell and Norman, 1998):

$$T_l = T_a + \frac{\gamma^*}{s+\gamma^*}\left[\frac{R_{int}}{g_{Hr}c_p} - \frac{VPD}{P_a\gamma^*}\right] \quad (1)$$

where Pa is the atmospheric pressure (kPa), VPD is the vapor pressure deficit (kPa), s is the slope of the saturation mole fraction [$\frac{\Delta}{Pa}$, being Δ the slope of the saturation vapor pressure function (kPa °C^{-1})], g_{Hr} is the convective-radiative conductance ($g_{Hr} = g_{Ha} + g_r$; mol m^{-2} s^{-1}, where g_{Ha} is the boundary layer conductance for heat, g_r is the radiative conductance), γ* is the apparent psychometric constant ($\gamma^* = \frac{\gamma g_{Hr}}{g_s}$, °C^{-1}). On each time-step, the model computes g_s, leaf transpiration (E_l, mol m^{-2} s^{-1}), leaf water potential (Ψ, kPa), net photosynthesis (A_n, μmol

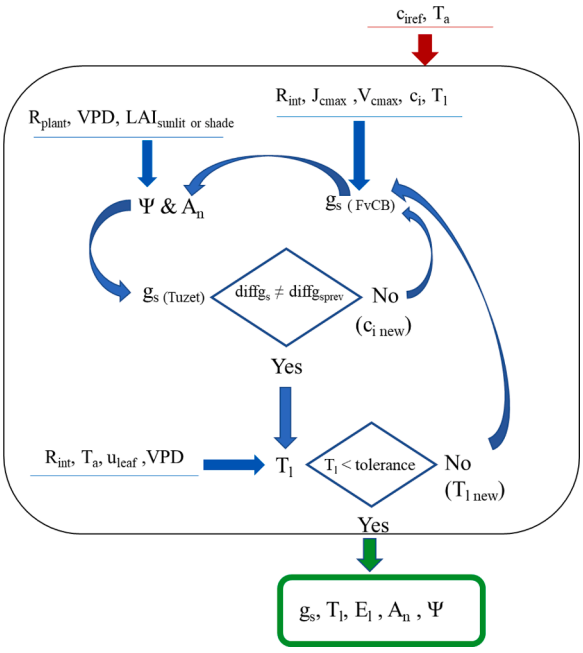

Fig. 1. The loop to model stomatal conductance (g_s), leaf temperature (T_l), leaf transpiration (E_l), net photosynthesis (A_n), and water potential (Ψ) for each leaf fraction, sunlit or shaded. Arrows represent the inputs to initialize the loop (red), outputs (green), and loop's sequence (blue). The loop works as follows. First, potential stomatal conductance ($g_{s\ (FvCB)}$) is estimated based on intercepted radiation (R_{int}), air temperature (T_a), photosynthesis limitation by the maximum rate of electron transport (J_{cmax}) or maximum rate of carboxylation (V_{cmax}), and an initial value for the internal concentration of CO_2 at the substomatal cavity ($c_{i\ ref}$). Second, g_s (FvCB), $c_{i\ ref}$, and the atmospheric CO_2 are used to obtain a first value of A_n. The $g_{s\ (FvCB)}$ is also combined with the plant resistance (R_{plant}), the LAI of the corresponding leaf fraction (sunlit or shaded), and the vapor pressure deficit (VPD) to obtain a first value of the leaf water potential (Ψ). A_n, Ψ and $c_{i\ ref}$ are then used to estimate a new g_s using Tuzet et al. (2003) approach [$g_{s\ (Tuzet)}$]. The actual difference $g_{s\ (Tuzet)}$ - $g_{s\ (FvCB)}$ ($diffg_s$) is compared with the previous difference ($diffg_{sprev}$). If the sign in $diffg_s$ differs from the sign in $diffg_{sprev}$, a solution is found, otherwise, the c_i is updated (c_{inew}) and the loop starts again. Once a solution for g_s is derived from the first loop, the temperature loop is initialized with R_{int}, air temperature (T_{air}), wind velocity at the top of the canopy (u_{leaf}), VPD, and $g_{s\ (Tuzet)}$. If the tolerance criteria for T_l is not met, the process starts again from the beginning updating Vcmax and Jmax with the new leaf temperature ($T_{l\ new}$) and computing a new $g_{s\ (FvCB)}$. Tolerance criteria is set to 0.1 °C. The R_{int} correspond to the PAR fraction intercepted by the canopy. In the model we assumed that radiation intercepted approximates to radiation absorbed, since leaves' radiation absorption in the PAR range is typically around 80% (Campbell and Norman, 1998).

$m^{-2}\ s^{-1}$) and T_l. Fig. 1 illustrates the inputs, outputs, and the loop used to close the leaf energy balance.

2.2. Model testing

The model has previously been tested for E_p and Ψ_{stem} in almond and olive trees (Garcia-Tejera et al., 2017a, 2017b). To explore the heatwave effect on grapevines, we 1) compared actual and modeled T_l and E_p, and 2) analyzed the sensitivity of T_l against theoretical expectations. Parameters to test the model were taken from the literature (Table 1) except those defining the orchard characteristics. Values to reduce g_s as a function of Ψ_{leaf} in Tuzet's model (Tuzet et al., 2003), were extracted from Levin et al. (2019) for *Vitis vinifera* L. 'Tempranillo'. Photosynthesis parameters for Farquhar's equation were obtained from Buckley et al. (2014) for 'Tempranillo' sunlit leaves. Minimum g_s was obtained from Duursma et al. (2019) and the xylem conductivity was from Choat et al. (2010). The root-specific hydraulic conductivity was from Gambetta

Table 1
List of values, units, and source of all parameters to test the model.

SYMBOL	DESCRIPTION	VALUE	UNIT	SOURCE
Root, Soil, and Xylem				
L_w	Leaf width	0.1	m	Study site
L_p	Root radial specific conductivity	8e-8	kg s^{-1} m^{-1} kPa^{-1}	Gambetta et al. (2012)
a_{root}	Root radius	0.001145	m	Reingwirtz et al. (2021)
SWA	Sapwood area	5.54e-04	m^2 sapwood tree $space^{-1}$	Study site
H	Trunk height (ground to the cordon)	0.9	m	Study site
h_{top}	Top of the canopy (from the ground)	2.13	m	Study site
K_h	Trunk specific hydraulic conductivity	0.0036	kg s^{-1} m^{-1} kPa^{-1}	Choat et al. (2010)
k_s	Soil saturated conductivity	0.00019	kg s m^{-3}	Campbell and Norman (1998)
Ψ_e	Air entry water potential	−2.1	kPa	Campbell and Norman (1998)
b	Shape factor	4.7	Dimensionless	Campbell and Norman (1998)
D	Soil layer depth	0.2	m	From Lv derivations treatment
$\acute{a}$	$1/L_p$ at which $\theta/\theta_s = \delta$	2	Dimensionless	Bristow et al. (1984)
β	The rapidity with which$1/L_p$ approach to infinity	30	Dimensionless	Bristow et al. (1984)
δ	The critical θ/θ_s at which $1/L_p$ becomes limiting	0.25	Dimensionless	Bristow et al. (1984)
F_{wet}	Fraction of soil area wetted by the emitter	20	Dimensionless	Study site
Dx	Alley distance	3	m	Study site
Dy	Row distance	1.7	m	Study site
θ_{pwp}	Soil water content at permanent wilting point	0.11	m^3 m^{-3}	Campbell and Norman (1998)
θ_{fc}	Soil water content at field capacity	0.24	m^3 m^{-3}	Campbell and Norman (1998)
θ_{sat}	Soil water content at saturation	0.43	m^3 m^{-3}	Campbell and Norman (1998)
Canopy				
C_a	External concentration of CO_2	420	micromol mol^{-1}	(NOAA, 2016)
g_o	Nighttime stomatal conductance for CO_2 at null gross photosynthesis	0.03	molCO_2 m^{-2} s^{-1}	Duursma et al. (2019)
m_p	Proportionality factor between photosynthesis and stomatal conductance	3.15	Dimensionless	*Derived from optimal g_s
Ψ_f	Water potential at half of maximum stomatal conductance	−1550	kPa	Levin et al. (2019))
sf	Shape factor	0.064	kPa^{-1}	Levin et al. (2019))
Photosynthesis				
θ'	Degree of curvature of the response to PAR to the electron transport rate	0.9	Dimensionless	Buckley et al. (2014)
f	fraction of absorbed photons that do not	0.2	Dimensionless	Buckley et al. (2014)

(*continued on next page*)

Table 1 (*continued*)

SYMBOL Root, Soil, and Xylem	DESCRIPTION	VALUE	UNIT	SOURCE
	contribute to photochemistry			
cK_c	Michaelis constant for CO_2. Scaling constant	38.05	Dimensionless	Buckley et al. (2014)
$\Delta H_a K_c$	Michaelis constant for CO_2. Activation energy	79.43e3	J mol^{-1}	Buckley et al. (2014)
cK_o	Michaelis constant for O_2. Scaling constant	20.3	Dimensionless	Buckley et al. (2014)
$\Delta H_a K_o$	Michaelis constant for O_2. Activation energy	36.38e3	J mol^{-1}	Buckley et al. (2014)
$c\Gamma$	CO_2 compensation point. Scaling constant	19.02	Dimensionless	Buckley et al. (2014)
$\Delta H_a \Gamma$	CO_2 compensation point. Activation energy	37.83e3	J mol^{-1}	Buckley et al. (2014)
cV_{cmax}	Maximum catalytic activity of Rubisco in the presence of saturating amounts ribulose biphosphate and CO_2. Scaling constant	28.73	Dimensionless	Buckley et al. (2014)
$\Delta H_a V_{cmax}$	Maximum catalytic activity of Rubisco in the presence of saturating amounts ribulose biphosphate and CO_2. Activation energy	59.454e3	J mol^{-1}	Buckley et al. (2014)
cJ_{cmax}	Maximum rate of electron transport. Scaling constant	16.83	Dimensionless	Buckley et al. (2014)
$\Delta H_a J_{cmax}$	Maximum rate of electron transport. Activation energy	30.201e3	J mol^{-1}	Buckley et al. (2014)
cR_d	Rate of CO_2 evolution in the light resulting from a process other than photorespiration. Scaling constant	18.72	Dimensionless	Buckley et al. (2014)
$\Delta H_a R_d$	Rate of CO_2 evolution in the light resulting from a process other than photorespiration. Activation energy	46.39e3	J mol^{-1}	Buckley et al. (2014)

Prefix ΔH_a and c in the photosynthesis parameters section correspond to the activation energy and scaling constant used to consider the temperature dependence of the parameters (Bernacchi et al., 2001). *m_p was derived by fixing all the parameters of Tuzet's model and assuming no water stress ($f_w = 1$).

Table 2
Vineyard characteristics in the modelling experiments at Raïmat and Nuriootpa.

Location	Row orientation	Trellis	Canopy height*	Canopy width	LAI
Raïmat	North-South	VSP	1.5	0.8	2
Nuriootpa	East-West	Single wire	1.6	1.7	2

* green area in the z direction.

Table 3
Maximum daily air temperature (T_{max}), vapor pressure deficit (VPD), and average daily wind velocity (U) of the heat wave used in the simulations.

Day	Tmax (°C)	VPD (kPa)	U (m s^{-1})
1	34.8	4.2	4.0
2	37.4	4.8	1.7
3	39.3	5.8	1.1
4	39.2	5.8	1.2
5	37.0	4.8	2.1
6	35.0	4.3	2.2

et al. (2012) for the R110 rootstock. Parameters for the reduction of root-specific hydraulic by soil drying were from Bristow et al. (1984). The soil characteristics were from Campbell and Norman (1998) for a silt loam soil. Other model parameters were measured at the study site described in next section.

2.2.1. *Measurement of plant transpiration, canopy temperature and model parameters in an established vineyard*

We measured vine transpiration and canopy temperature to test the model (Table 1). Measurements were made in a commercial vineyard at Raïmat (Lleida, Spain, 41.69°N; 0.49 °E) during the 2019 growing season. The vines were 22-years old 'Tempranillo' grafted on R110 and planted at 1.7 × 3.0 m. Vines were cordon-trained through a vertical shoot positioning (VSP) trellis system, with a bilateral, spur-pruned cordon located at a height of 0.9 m above ground. Disease control and vine nutrition management followed local practices in the region.

Two irrigation treatments were established to broaden the range of transpiration and canopy temperature to overlay the seasonal variation of these traits. Irrigation was performed from 1st April to 1st September (treatment I_1), and from 1st April until 15th May (treatment I_2). Each treatment was imposed to 41 vines, with each single vine representing an experimental unit. Water was applied 2–3 days per week through drip irrigation with two drippers per vine and with a discharge rate of 4 l h^{-1}. A water meter (CZ2000–3 M Contazara, Zaragoza, Spain) was installed on the dripline to measure the volume of irrigation water applied. Vine water requirements were calculated with a water balance to replace crop evapotranspiration. Crop evapotranspiration was calculated from the ET_0 of Penman-Monteith (Allen et al., 1998) and crop coefficients derived from previous experiments (Olivo et al., 2008). Crop coefficients ranged from 0.5 at fruit-set to 0.7 at harvest. The total amount of irrigation water applied was 223 mm for I_1 and 47 mm for I_2. Rainfall during the season was 331.4 mm

Leaf area index (LAI) was obtained multiplying canopy volume by leaf area density. The leaf area density was obtained through defoliation of four plants in the same vineyard. Before defoliation, canopy volume was measured. Once defoliated, we collected a sample of 100 leaves to measure the area with a leaf area meter (LI-3100C, LiCor Lincoln, NE, USA). Finally, all the leaves were dried at 60 °C until constant weight. The relation between leaf area and weight from the 100 leaves sample was used to estimate the total plant leaf area from leaf weight. The leaf area : canopy volume ratio was used to obtain the leaf area density. Canopy volume was measured seven times during the season, from May 9th to August 23rd, assuming a rectangular shape. Leaf area index (LAI) peaked at 1.6 for I_1 and 1.4 for I_2.

Grapevine E_p was estimated in 2 vines per irrigation treatment with a sap flow system using the compensated heat-pulse method (Swanson and Whitfield, 1981) combined with the calibrated average gradient method (Testi and Villalobos, 2009). Probes were placed 30 cm above the ground and shielded to avoid errors due to radiative or convective heating of the system. Probes, developed at the IAS-CSIC laboratory, consisted of a 4.8-W stainless steel heater of 2 mm diameter and two temperature sensors located 10 and 5 mm down and upstream of the heater, respectively (Testi and Villalobos, 2009). Each temperature sensor had two embedded type E (chromel–constantan wire) thermocouple junctions, spaced 10 mm along the needle, that were sampled

Table 4
Canopy attributes of the four treatments used in the shoot trimming simulation.

Location	Orientation	Treatments Trellis	Trimming	Canopy height (m)	Canopy width (m)	LAI
Raïmat	North-South	VSP	no	1.5	0.8	2
			yes	1.0	0.8	1.3
Nuriootpa	East-West	Single wire	no	1.65	1.5	2
			yes	1.65	1.0	1.4

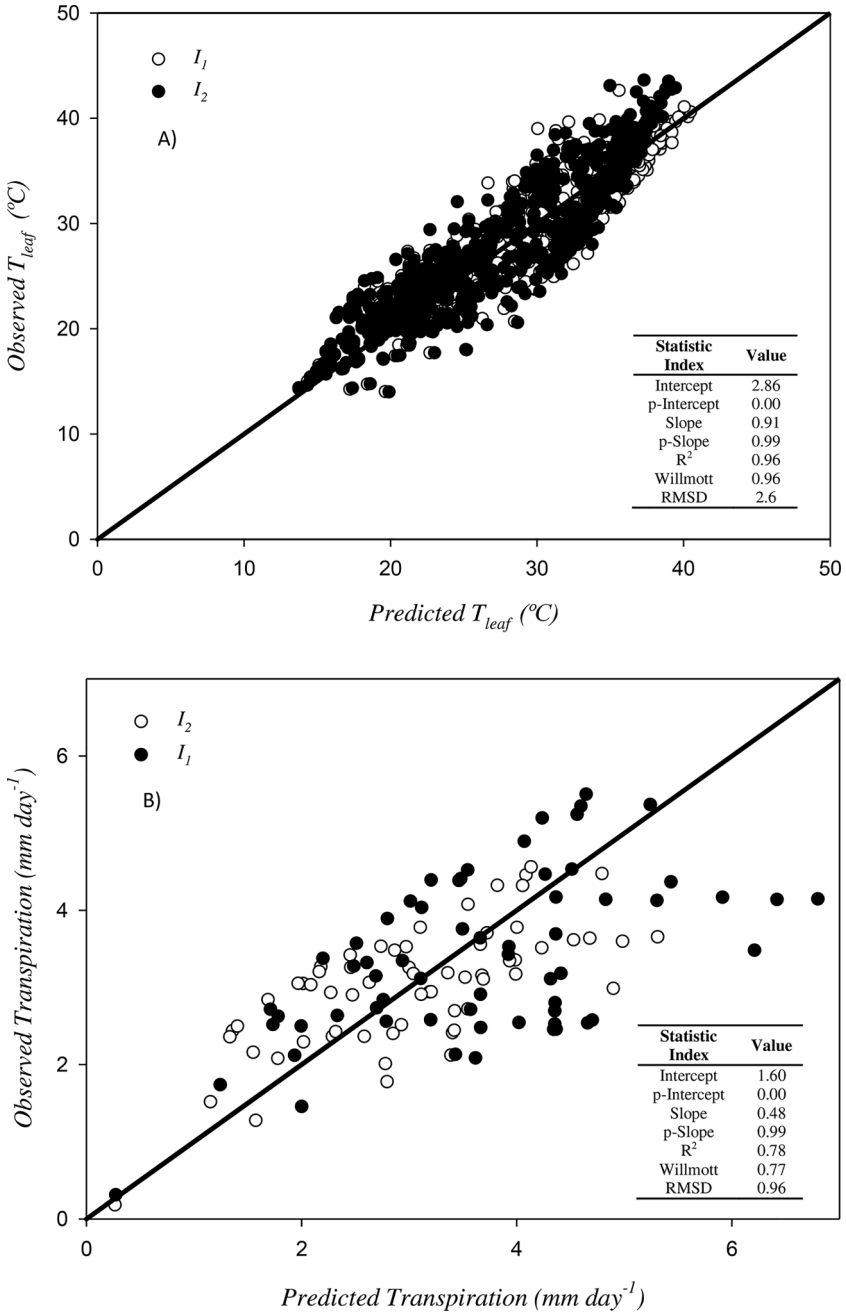

Fig. 2. Comparison of observed and predicted A) sunlit leaf temperature (T_{leaf}) and B) transpiration for fully-irrigated vines (I1) and vines only irrigated early in the season (I_2). The tables show the statistics of model performance including the intercept and slope of the regression between observed and predicted data, their corresponding p-values, the Willmott's index of agreement (Willmott, 1984), and the root mean square deviation (RMSD). Black lines are the identity lines.

separately to obtain heat-pulse velocities at 5 and 15 mm below the cambium. The system was controlled with a datalogger (CR1000, Campbell Scientifc Inc., Logan, UT, USA) and sampled at 15-min intervals. Heat-pulse velocities were corrected for wounding reactions (Green et al., 2003). The sap flow was derived by integration of sap flux densities, first, across the trunk radius and, then, around the azimuth angle (Green et al., 2003).

Sap flow records need to be corrected for the azimuthal variability of

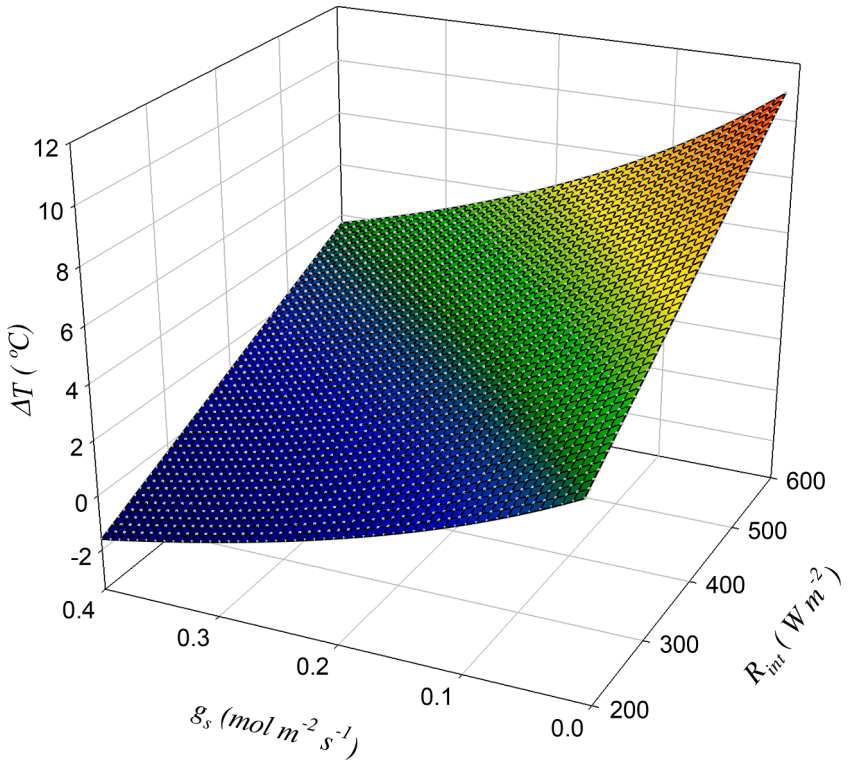

Fig. 3. Differences in daily temperature between canopy and air (ΔT) as a function of (A) stomata conductance (g_s) and intercepted radiation (R_{int}). Simulations have been performed for air temperature = 35 °C, U = 5 m s^{-1}, and RH = 30%.

sap flow rates (López-Bernal et al., 2010). We performed a specific calibration of each sap flow sensor using a gas exchange open chamber (Corelli-Grappadelli and Magnanini, 1993). The chamber volume was around 4.7 m^3 and was built using mylar® plastic with a light transmittance of 90% and low water absorbance and carbon dioxide permeability (manufacturer technical sheet). Air entering the chamber was sampled from a 3.5 m tall aluminum pipe (20 cm diameter). A single 190 W centrifugal fan (Casals Ventilación Industrial IND, S.L., Girona, Spain) chamber was used to blow up the air into the chamber through a 19 cm diameter PVC pipe. An aluminum manifold parallel to the arms of the vine was used to distribute the air inside the chamber. Air mixing was enhanced by adding two 12 V CPU fans above the canopy. The air velocity was measured using an air velocity transmitter (Dwyer Series 641, USA). The calculated flow was calibrated against air volume measured using the pure CO_2 dilution method once in the laboratory prior to development (Wünsche and Palmer, 1997). Airflow was fixed at around 12 m^3 min^{-1} using a fan velocity regulator REG-5 (Casals Ventilación Industrial IND, S.L., Girona, Spain). Reference parameters were continuously measured inside and outside the chamber; temperature and relative humidity were monitored using a Vaisala HMP110 sensor (Vaisala Corporation, Helsinki, Finland) and global solar radiation was measured with a pyranometer (Apogee SP-110, Apogee Instruments, Inc., North Logan, USA). Ambient H_2O concentrations in the inlet (H_2O reference) and at the chamber's outlet (H_2O sample) were measured by an infrared gas analyzer (Li-6400, Li-Cor, Inc., Lincoln, NE, USA).

Effective sunlit leaf temperature was recorded every 5 min using two infrared radiometers (SI-121, Apogee Instrument inc, Logan, UT, USA), one per irrigation treatment, pointing to leaves in the upper part of the canopy. Infrared radiometers were installed about one meter above, positioned with 45º angle and ensuring that the targeted area was pure canopy. The radiometers have a narrow 18º half-angle field of view and a response of 0.6 s.

Root biomass was measured in two nearby grapevines. For each plant, soil cores were extracted every 0.2 m to a depth of 1.2 m, coinciding with the presence of a calcareous layer that prevented deeper root growth. The coring and sampling were repeated at three positions perpendicular to the vine row at a distance of 0.25, 0.5, and 0.75 m towards the midrow space to obtain the spatial distribution of root biomass. Root biomass was converted to root length density (m_{root} m_{soil}^{-3}) using the specific root length reported by Reingwirtz et al. (2021) for an R110 rootstock.

2.2.2. Statistical analysis of model performance and sensitivity analysis

To analyze model performance we compared observed vs predicted traits (Piñeiro et al., 2008) and derived Willmott's index of agreement (Willmott, 1984). Willmott's index rate model's prediction error using a score from 0 (no agreement at all) to 1 (perfect match). The Willmott's index is calculated comparing observed (O), predicted (P), and the average of observed ($\overline{O}$) values.

$$d = 1 - \frac{\sum_{i=1}^{n}(O_i - P_i)^2}{\sum_{i=1}^{n}(|P_i - \overline{O}| + |O_i - \overline{O}|)^2} \quad (2)$$

Model sensitivity analysis was performed by varying one or two parameters on Eq. (1) at a given time, and by analyzing the response on the difference between canopy and air temperatures (ΔT). The selected parameters were stomata conductance (g_s), radiation interception (R_{int}), wind velocity (U), and relative humidity (RH). The range of values was selected from the observed data in the validation experiment (Section 2.2.1).

2.3. Modelling the impact of management practices on vine transpiration, stem water potential, and canopy temperature

We modeled vine transpiration, stem water potential and ΔT in response to the interaction between radiation load and other factors including soil water content, wind speed and leaf size. We targeted two locations: Nuriootpa, Barossa Valley, South Australia (34 °S, 139 °E), and Raïmat, Costers del Segre, Spain (41.69 °N; 0.49 °E). The sites share Mediterranean-type climate (di Castri and Mooney, 1973). According to

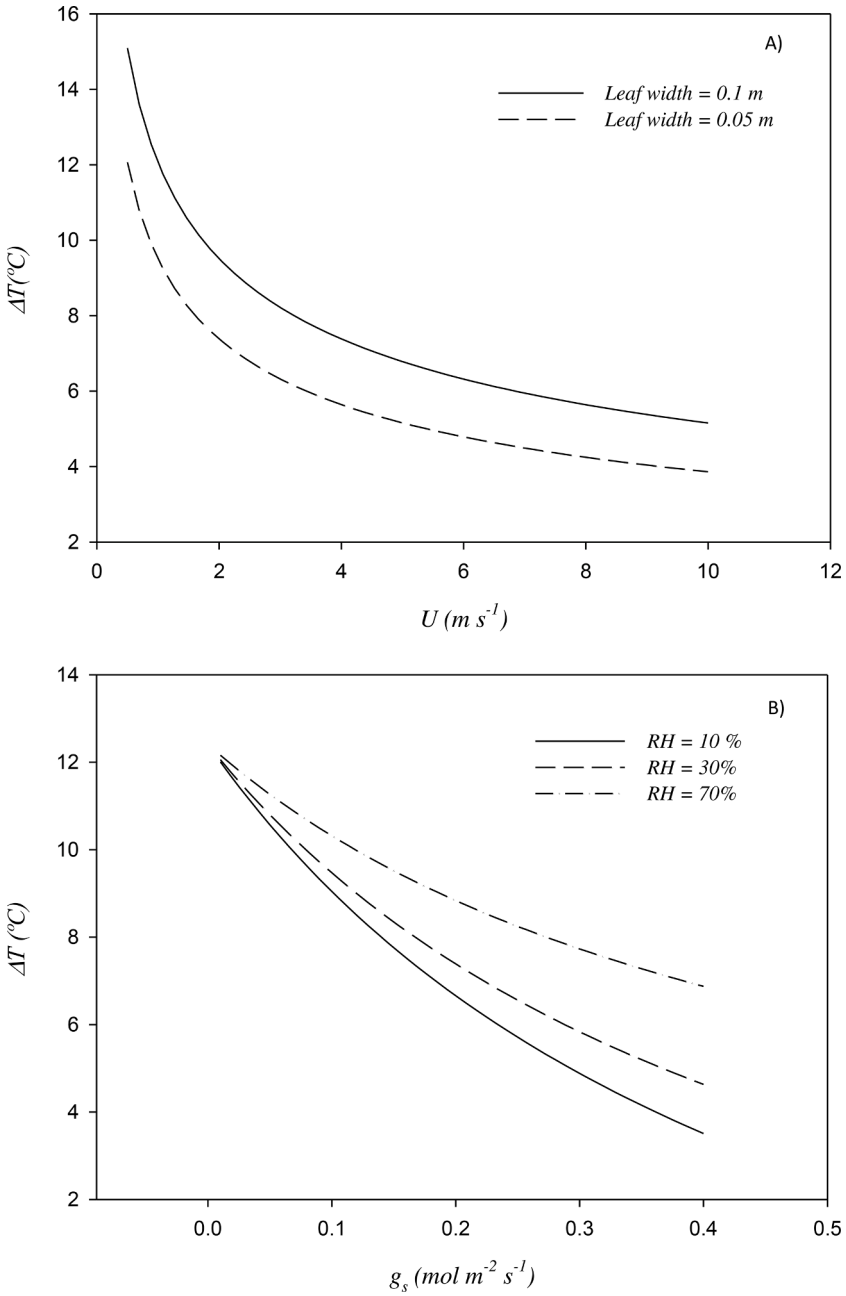

Fig. 4. Differences in daily temperature between canopy and air (ΔT) as a function of (A) wind velocity (U) and leaf width, and (B) stomatal conductance and relative humidity (RH). Simulations have been performed for air temperature = 35 °C, U = 2 m s^{-1} (B), R_{int} = 600 W m^{-2} (A and B), $g_{s=}$ 0.2 mol m^{-2} s^{-1} (A) and RH = 30% (A).

Köppen-Geiger (Kottek et al., 2006), Raïmat is a Cfb region with a warm temperature and hot summer, whilst Nuriootpa is Csb with a warm temperature and hot and dry summer. Table 2 summarizes vineyard characteristics used in modelling. In Nuriootpa, row orientation was E-W with vines allowed sprawl from a single cordon, a fixed wire 0.4 m from the cordon helped support the shoots. In Raïmat, vineyard orientation was N-S and the canopy was managed using VSP. Canopy size was 1.6 m high x 1.7 m wide in Nuriootpa, and 1.5 m high x 0.8 m wide in Raïmat. LAI was set to 2 m^2 leaf m^{-2} soil in both sites. Other input parameters for the model are listed in Table 1

For a given management practice, a range of water stress was generated by varying soil water content in allthe soil layers from field capacity (Ψ_{soil} = −33 kPa) to wilting point (Ψ_{soil} = −1500 kPa). Soil water content was expressed as the total fraction of available water (TFAW) using Campbell's soil moisture release equation (Campbell, 1985)

$$TFAW = \frac{\theta_{act} - \theta_{pwp}}{\theta_{fc} - \theta_{pwp}} \quad (3)$$

where, θ is soil water content, and subscripts indicate actual (*act*), field capacity (*fc*), and permanent wilting point (*pwp*).

For the characterization of heatwaves, we used available historical daily averages from nearby weather stations from 1990 to 2019 in Raïmat and from 1997 to 2020 in Nuriootpa (BoM, 2016; RuralCat, 2020). These periods capture the World Meteorological Organisation's updated definition of 'present-day' climate formally represented by the meteorological statistics of the period 1991–2020 (Hulme, 2020); climate change projections were beyond the scope of this study. Year difference between sites resulted from data availability. We defined a

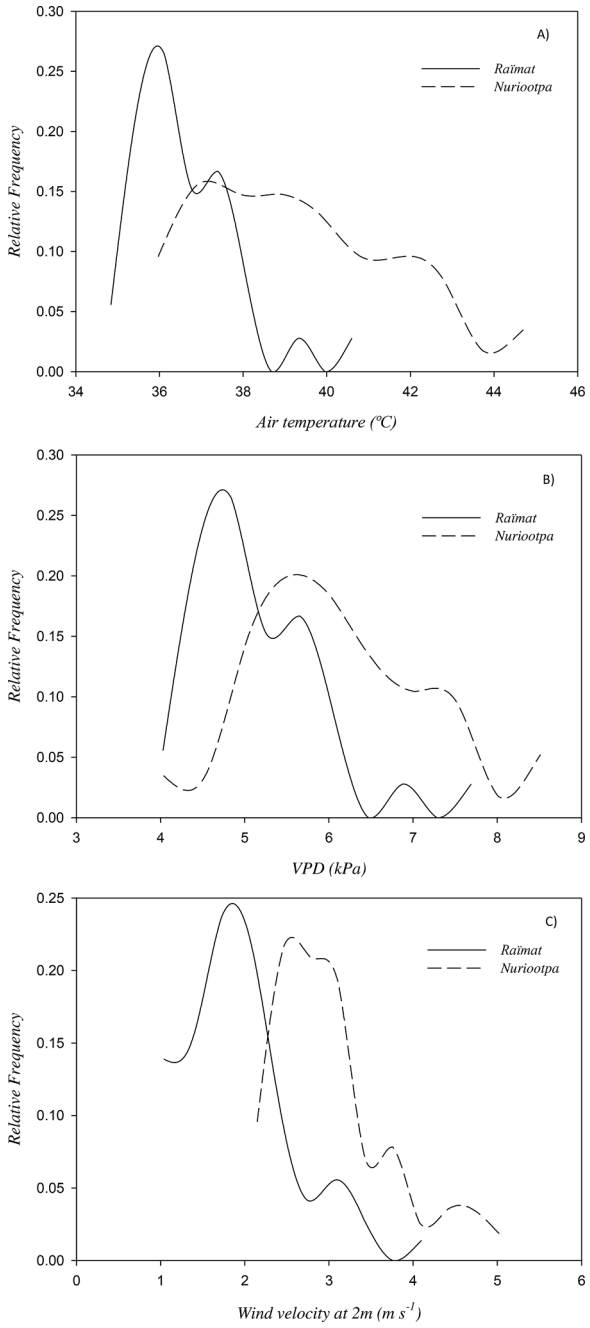

Fig. 5. Frequency distribution of (A) maximum air temperature, (B) wind velocity, and (C) vapor pressure deficit during a heatwave at Raïmat, Spain, (41.68°N, 6.44° E) and Nuriootpa, South Australia, (34 °S, 139 °E). The analysis corresponds to 29 years (from 1990 to 2019) for Raimat and 23 years (from 1997 to 2020) for Nuriootpa.

heatwave as either five consecutive days with maximum daily temperature above 35 °C or three consecutive days with maximum daily temperature above 40 °C (Grace et al., 2009). Once the heatwave events were identified, we analyzed the frequency distributions of air temperature (T_a), vapor pressure deficit (VPD), and wind speed at each location to generate a virtual heatwave event that would be realistic for both sites (Table 3).

2.3.1. Baseline

We modelled vine transpiration, water potential, and canopy temperature during a heatwave (Table 3) at Raïmat and Nuriootpa to establish a baseline using the parameters in Tables 1 and 2.

2.3.2. Reduction of radiation load

We explored the effect of reductions in R_{int} through row orientation, shade cloth, kaolin application and canopy trimming. For kaolin application, we assumed a perfect distribution of the product on the leaf surface of the entire canopy and no-blockage of stomata (Rosati et al., 2006). The change in leaf reflectance used to model the kaolin effect was obtained from Shellie and King (2013). For the shade cloth, we simulated an overhead system that excludes 50% of the direct sunlight and allows lateral air circulation (Caravia et al., 2016). We assumed shade cloth did not change air temperature, relative humidity, and wind speed. Canopy trimming was tailored to the specific trellis system of each location (Table 4). At Raïmat with a VSP trellis, we assumed topping that reduced initial canopy height 0.5 m, from 1.5 to 1.0 m. At Nuriootpa, with the sprawling canopy, we assumed a lateral trimming of each side, reducing the overall canopy width 0.5 m, from 1.7 m to a 1.2 m. The rest of the inputs were the same as in Tables 1 and 2.

We explored the effects of a heatwave on canopy temperature by changing row orientation under different fractions of soil available water. We use the same experimental settings at each site as in the baseline (Section 2.3.1) and defined row orientation as NS, EW, NE-SW, and NW-SE.

3. Results

3.1. Model testing

Fig. 2 compares predicted and observed T_l and E_p. The Willmott coefficient was 0.96 for T_l and 0.77 for E_p. There was consistency between observed and predicted values (p for slope > 0.05), which indicates that the model can reproduce variations on both T_l and E_p. Positive intercepts ($p < 0.05$) indicates model bias for both traits (Piñeiro et al., 2008).

At a g_s of 0.4 mol m^{-2} s^{-1}, which may be expected for a well-watered vine, canopy temperature varied from a cooling of ~ 1.6 °C to an increase of ~ 3.7 °C relative to the ambient air temperature in response to an increase in R_{int} from 200 to 600 W m^{-2}. At a g_s of 0.01 mol m^{-2} s^{-1} representing a water-stressed vine, the ΔT increased from 3.5 °C at 200 W m^{-2} to 10.9 °C at 600 W m^{-2} above the ambient air temperature (Fig. 3). Irrespective of leaf size, ΔT declined non-linearly with wind speed, and modeled canopy temperature approached air temperature, i.e., ΔT → 0, at higher wind speeds (Fig. 4A). This is the result of an increase in the boundary layer conductance, as the wind generates turbulence that reduces the boundary layer thickness (Monteith and Unsworth, 2013). On the contrary, at low wind velocity, there was a decoupling of the leaf temperature, increasing ΔT. The model does not account for a change from forced to free convection, which explains the sharp increase in ΔT at low wind velocities (Monteith and Unsworth, 2013). With increasing wind speed from 0.5 to 10 m s^{-1}, ΔT varied from 15.0 °C to 5.2 °C for 0.1 m leaf width, and from 12.0 °C to 3.8 °C for 0.05 m leaf width. The effect of leaf size was larger at lower wind speed: larger leaves were 3.0 °C hotter than their smaller counterparts at U = 0.5 m s^{-1}, and 1.3 °C hotter at 10 m s^{-1} (Fig. 4A). As g_s decreases so does ΔT regardless of the RH; however, the drop is sharper under low RH (< 30%) than at high RH (70%) (Fig. 4B).

3.2. Characterization of heatwaves in Raïmat and Nuriootpa

In Raïmat, the maximum daily temperature (T_{lmax}, °C) during the heatwave rarely exceeded 39 °C. The most common heatwave event had a temperature of around 36 °C for 5 days. In Nuriootpa, the relative frequency of T_{lmax} was more evenly distributed, with maximum frequencies ranging from 36 °C to 39 °C (Fig. 5A). The VPD followed a similar pattern; in Raïmat the maximum VPD frequency was around 4.5 kPa, whereas in Nuriootpa the VPD during a heatwave peaked at 5.5 kPa and 7.5 kPa (Fig. 5B). The wind speed during a heatwave was slightly higher in Nuriootpa than in Raïmat (Fig. 5C). In Raïmat, the maximum

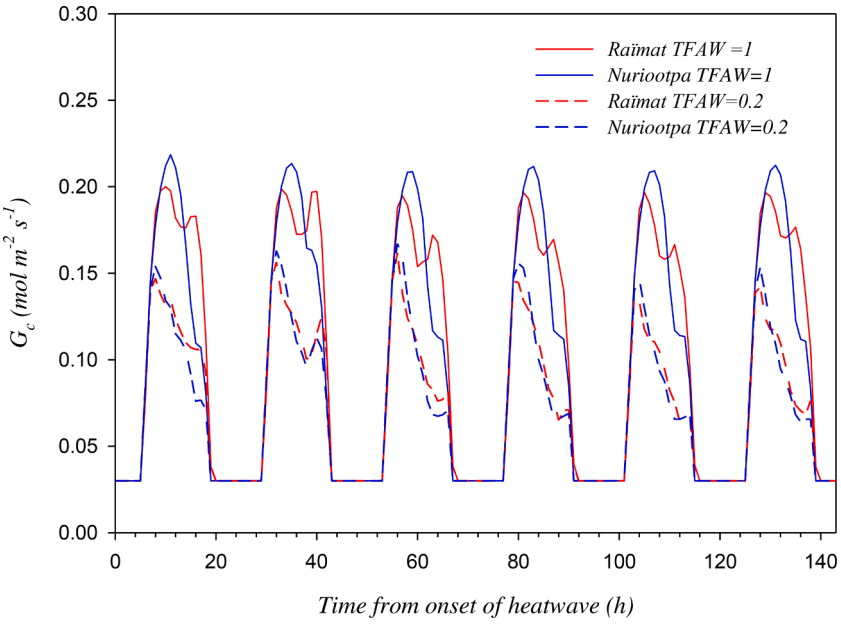

Fig. 6. Dynamics of canopy conductance (G_c) during the heatwave at Raimat and Nuriootpa in dry (TFAW = 0.2) and wet soil (TFAW = 1).

frequency was between 1.5 and 2 m s^{-1}. In Nuriootpa, this maximum was between 2.5 and 3 m s^{-1}.

3.3.1. Baseline

The evolution of canopy conductance (G_c) varied with location and TFAW. The model captured the lower conductance in drier soil, TFAW = 0.2 compared to TFAW = 1 (Fig. 6). In Nuriootpa, with an EW orientation and a single wire trellis, the G_c peaked early in the morning and decreased towards the afternoon. In Raïmat, with an NS orientation and a VSP trellis, G_c showed two daily peaks, one in the morning and another in the afternoon; the difference between the morning and afternoon peaks increased with the progression of stress during the heatwave (Fig. 6). Despite the differences in G_c, the evolution of the minimum relative stem water potential was the same in both locations (Fig. 7A). At a TFAW = 0.04 the minimum stem water potential was 3.5 times greater than at a TFAW = 1. The piecewise function fitted across sites and treatments on the relationship between T_{lmax} and soil moisture indicates an increase in T_{lmax} of around 1 ºC for each 10% reduction in soil moisture from field capacity to TFAW = 0.4, and a steeper increment in T_{lmax} of around 10 ºC for each 10% of soil drying from TFWA between 0.4 and 0.2 (Fig. 7B).

3.3.2. Interaction between radiation load and water stress

Incident radiation was modified with row orientation, shade cloth covering the canopy, kaolin application to the canopy, and shoot trimming before a heatwave.

Row orientation. Row orientation impacted on T_{lmax} by affecting both R_{int} distribution throughout the day and the total R_{int}. Both R_{int} and T_{lmax} were higher in Raïmat than in Nuriootpa irrespective of row orientation. The variation in T_{lmax} with row orientation was small and ranged between 1.6 and 1.8 ºC through the simulated range of TFAW. The largest difference in T_{lmax} between row orientations was observed in dry soil. A high g_s in wet soil promoted E_p, dampening the differences in R_{int} and reducing the effect of row orientation (Fig. 8A and B).

At both sites, the NS orientation resulted in the highest canopy temperature (Fig. 8A and B). The orientation for the lowest canopy temperature varied between locations: it was NW-SE at Nuriootpa and NE-SW at Raïmat; with these orientations, canopies were 1.6 to 1.8 ºC cooler than the NS orientation. The R_{int} and T_{lmax} dynamics varied between sites. NS orientation at Raïmat produced two marked R_{int} peaks, before and after noon. The same orientation at Nuriootpa produced only one peak of R_{int} in the afternoon. These differences are the result of the training system; Nuriootpa had a sprawl trellis system characterized by a low wide canopy whereas, in Raïmat, the VSP trellis had a narrow, tall canopy.

Shade cloth and kaolin. We only considered the impact of kaolin and shade-cloth individually as it is unlikely that they would be used in combination in commercial vineyards. At both sites, as expected from the results above (Fig. 3), a reduction of R_{int} decreased T_{lmax}. The kaolin treatment lowered R_{int} by 20%, which compares to a 50% reduction using shade cloth, explaining the differences in T_{lmax} between treatments (Fig. 9A and B). The degree of cooling of each treatment differed between sites. In Raïmat, the shade cloth reduced T_{lmax} by 3.7 ºC on average across the range of TFAW, with a maximum cooling of 5 ºC at TFAW = 0.18. The kaolin had an average reduction of 1.1 ºC and a maximum cooling of 1.5 ºC at TFAW = 0.2 (Fig. 9A). In Nuriootpa, the kaolin had a greater impact than in Raïmat; the average reduction of T_{lmax} was 2 ºC for the kaolin and 3ºC for the shade cloth (Fig. 9B). The maximum cooling difference with the control was 2.6 ºC and 4.5 ºC for kaolin and shade cloth respectively, at TFAW = 0.18. Regardless of the treatment and site, the T_{lmax} increased with soil drying (Fig. 9A and B).

Trimming the canopy before a heatwave. Trimming lowered T_{lmax} but the degree of reduction changed with soil water content; for TFAW between 1 and 0.4; the difference in T_{lmax} between trimmed and untrimmed canopies was around −2 ºC (Fig. 10). For TFAW below 0.4, the difference between treatments increased sharply. At TFAW = 0.2 the maximum difference was −7.5 ºC in Nuriootpa and −7.0 ºC in Raïmat. For TFAW < 0.2, the difference in T_{lmax} decreased almost linearly until a minimum of −4º C in Raïmat and −3.5º C in Nuriootpa (Fig. 10). The shape of these curves (see Fig. 10) responds to the different weights of R_{int} and g_s after trimming when soil dried. When the soil water content was not limiting, g_s reached its maximum for the simulated weather, and the reductions in R_{int} accounted for the differences in T_{lmax}. As the soil dried and the stomata closed, the more favorable root-to-leaf area ratio and Ψ in trimmed vines contributed to maintaining g_s, counteracting the negative effect of reduced soil moisture on E_p. This coincides with the increase in the T_{lmax} difference between trimmed and untrimmed vines,

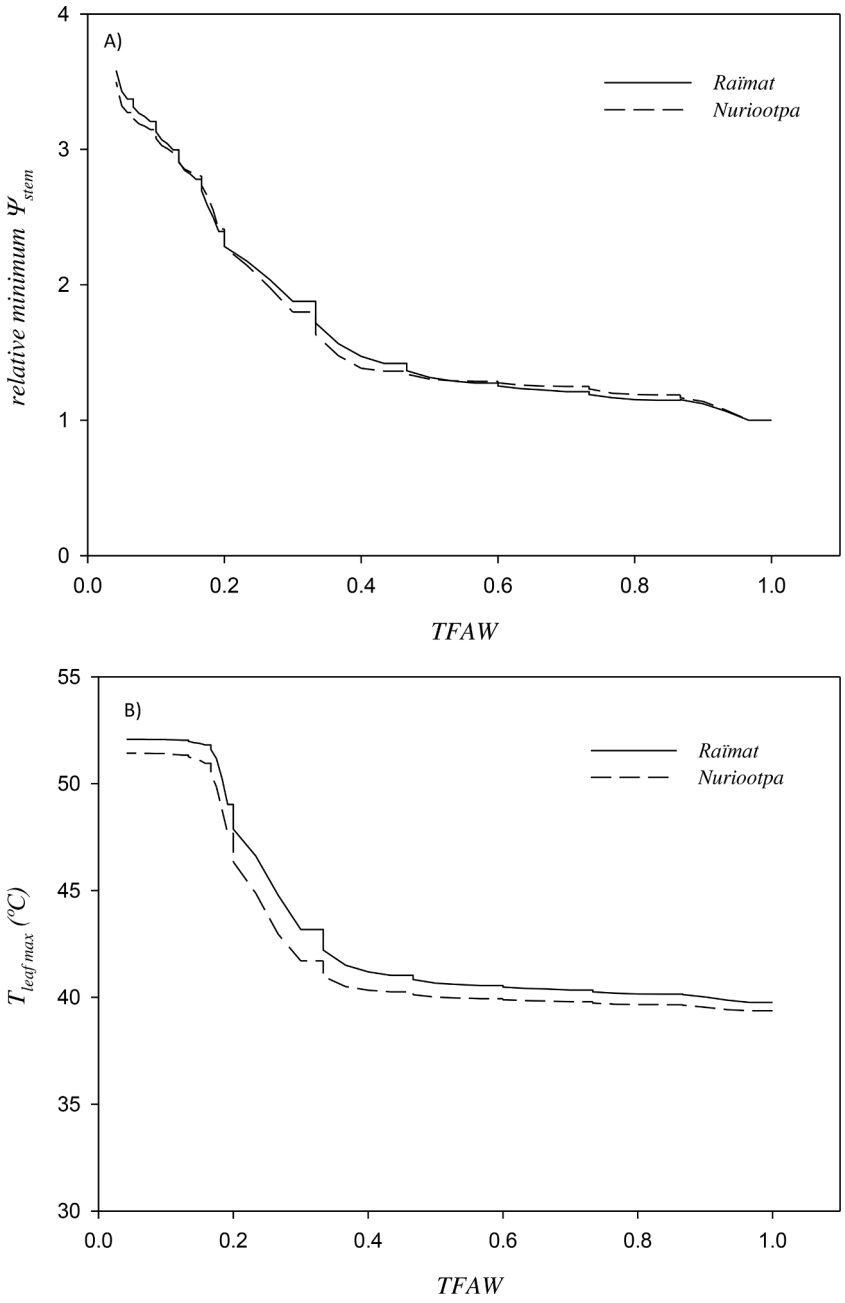

Fig. 7. A Change on relative minimum Ψ_{stem} - expressed as the ratio between the minimum water potential when the soil is at field capacity (TFAW=1) and the minimum water potential at the corresponding TFAW- during the heatwave at different soil water. B) ΔT_{max} as a function of soil water content.

between 0.4 and 0.2 TFAW. As the soil dried further, g_s became gradually lower overriding the positive effect of trimming on the root-to-leaf area ratio and Ψ. Consequently, the T_{lmax} difference diminished.

4. Discussion

4.1. . Model precision, accuracy, and sensitivity

Comparison of actual and modelled transpiration and canopy temperature indicated high model precision (Willmott's coefficient ≥ 0.77), and some bias (non-zero intercept) that may relate to model parametrization. Some model parameters feature high phenotypic plastic (DeWitt and Scheiner, 2004); for instance, root radial specific conductivity presents circadian variation (Caldeira et al., 2014; Vandeleur, 2007) and is responsive to water stress (North and Nobel, 1992, 1997; Vandeleur, 2007). The maximum catalytic activity of Rubisco with saturating amounts of ribulose biphosphate and CO_2 changes with leaf nitrogen content (Kattge et al., 2009; Wilson et al., 2000). This bias may have induced deviations in T_l between observations and predictions by the model (Fig. 2B). However, as indicated by the analysis of the slope and data scatter around the regressed function (P-slope=0.99, alfa=0.05), there was consistency between predicted and observed values indicating good predictability of T_l and E_p by variations of other variables.

The sensitivity analysis showed the responses of modelled T_l to the variables in Eq. (1). The model captured the trends in ΔT with R_{int} and g_s (Fig. 3), U (Fig. 4A), and RH (Fig. 4B) reported in the literature (Bellvert et al., 2015; Gonzalez-Dugo et al., 2020; Jackson et al., 1981). Owing to the influence of weather and plant traits on the relation between T_l and T_a (Fig. 3), particularly the dependence of g_s on R_{int}, T_l, and VPD

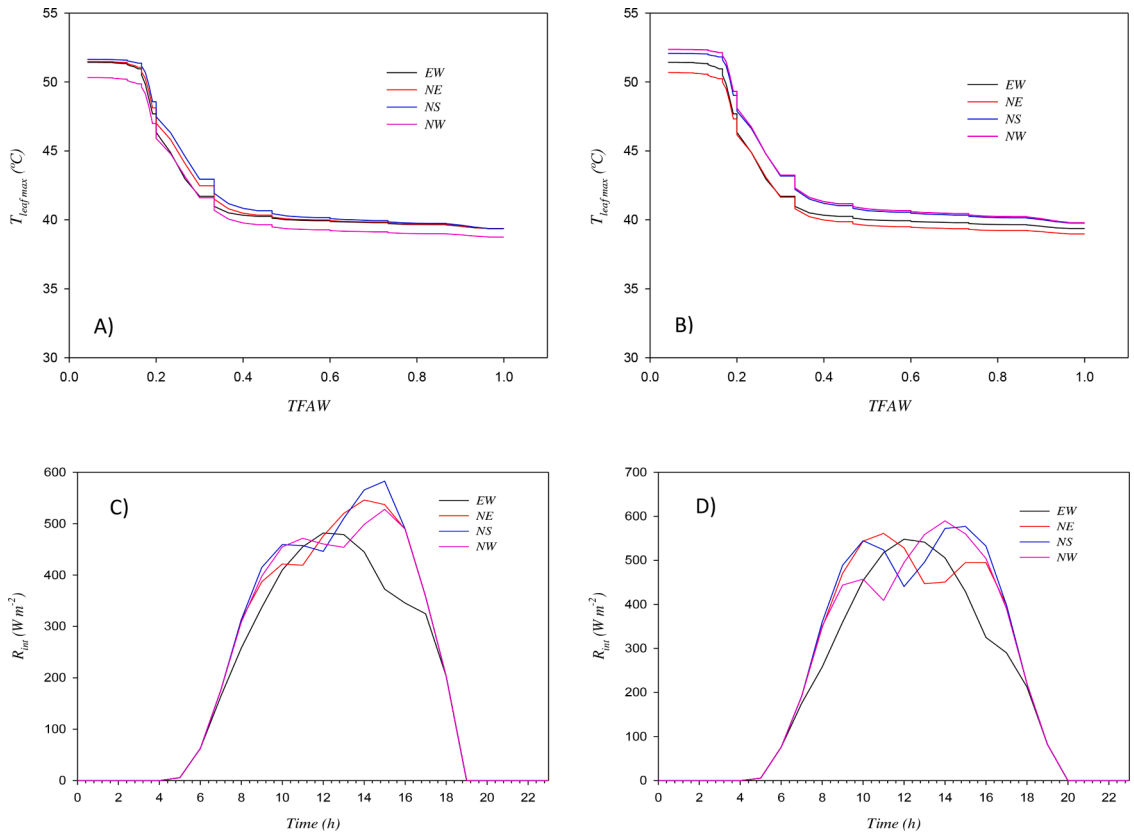

Fig. 8. (A, B) Effect of row orientation and total fraction of available water (TFAW) on maximum leaf temperature ($T_{leaf\ max}$). (C, D) Daily evolution of radiation interception (R_{int}) for different row orientations at Nuriootpa (Single wire) and Raïmat (VSP). Hours are on local time zone.

(Damour et al., 2010), we can expect departures between actual and modelled ΔT. To avoid this issue, our model computes T_l combining Eq. (1) with the g_s model (Fig. 1).

4.2. Agronomic limitations of temperature thresholds to define heatwaves

Air temperature interacts with other factors modulating canopy temperature (Jackson et al., 1981). For a given wind speed and VPD, canopy temperature is the result of the interaction between R_{int} and g_s (Fig. 3). However, Eq. (1) highlights the impact of wind speed and VPD on ΔT (Fig. 4A and B). Canopy temperature is the result of an infinite set of R_{int} x g_s planes, one per each combination of wind speed, VPD and air temperature during the heatwave. This challenges the scientific and agronomic relevance of definitions of heatwaves solely based on temperature thresholds – the biological effect of three days with maximum temperature above 35 °C will be completely different with high or low wind speed, or higher or lower VPD. The complete set of relevant weather conditions during a heatwave needs consideration in the assessment of management strategies.

The increase of g_s through irrigation will fail to reduce canopy temperature below critical values (Fig. 4B), when high relative humidity (low VPD) constrains plant transpiration (Villalobos and Fereres, 2017) and canopy cooling. Likewise, irrigation will have a lesser impact on canopy cooling in isohydric varieties such as Granache, that readily closes stomata in response to dry soil and high VPD, in comparison to Shiraz that maintains higher stomatal conductance (Soar et al., 2009). Reducing energy load in a vineyard with an already low R_{int} will have little effect on dampening heat wave effects, but it may compromise biomass production and yield (Greer et al., 2011). Therefore, practices should be tailored to account for the set of relevant weather, plant, management, and soil conditions driving canopy cooling.

4.3. Heatwave effects interacting with training system and row orientation

The combination of training system and row orientation influenced R_{int} and T_{lmax} (Figs. 7B and 8). However, Hunter et al. (2016) found that R_{int} changes due to row orientation in VSP trained grapevines did not produce a significant change in T_{lmax} and Ψ. The T_{lmax} in Fig. 8A and B resulted from the extreme temperatures during the simulations. Under such temperatures, slight changes in R_{int} will cause big shifts in T_{lmax}. On the contrary, the simulated change in Ψ (Fig. 7A) agreed with the results observed by Hunter et al. (2016) and Buesa et al. (2020) who compared different combinations of row orientations and varieties. In a review of hedgerow olive experiments with a focus on plant physiology, fruit quality, and yield, Trentacoste et al. (2015) showed trait-dependent response to row orientation. Fig. 8 illustrates that latitude and trellis influenced T_{lmax} at the same TFAW, despite using the same soil characteristics, root distribution, and LAI. Experiments and modelling converge to show that the impact of the vineyard layout on T_l is not straightforward. Preliminary analysis of the interaction between row orientation, trellis, climate and soil could inform decisions.

Field experiments with Shiraz in Barossa Valley and with Malbec in Mendoza, Argentina, showed that vines upregulate stomatal conductance, hydraulic conductivity, and transpiration in response to elevated temperature. Hence, acclimatation to heat mediated by evaporative cooling overrides stomatal regulation to sustain water use efficiency (Bonada et al., 2018; Galat Giorgi et al., 2020, 2019; Sadras et al., 2012; Soar et al., 2009). Similarly, stomatal regulation that favors evaporative cooling over water use efficiency has been associated with yield improvement in annual crops (Lu et al., 1994; Roche, 2015). Our simulations did not account for changes in g_s due to heat. In both sites, the parameters defining the g_s response to VPD and Ψ were the same. However, we found different g_s responses associated with the distribution of light (Fig. 6). The combination of variety response to heat and

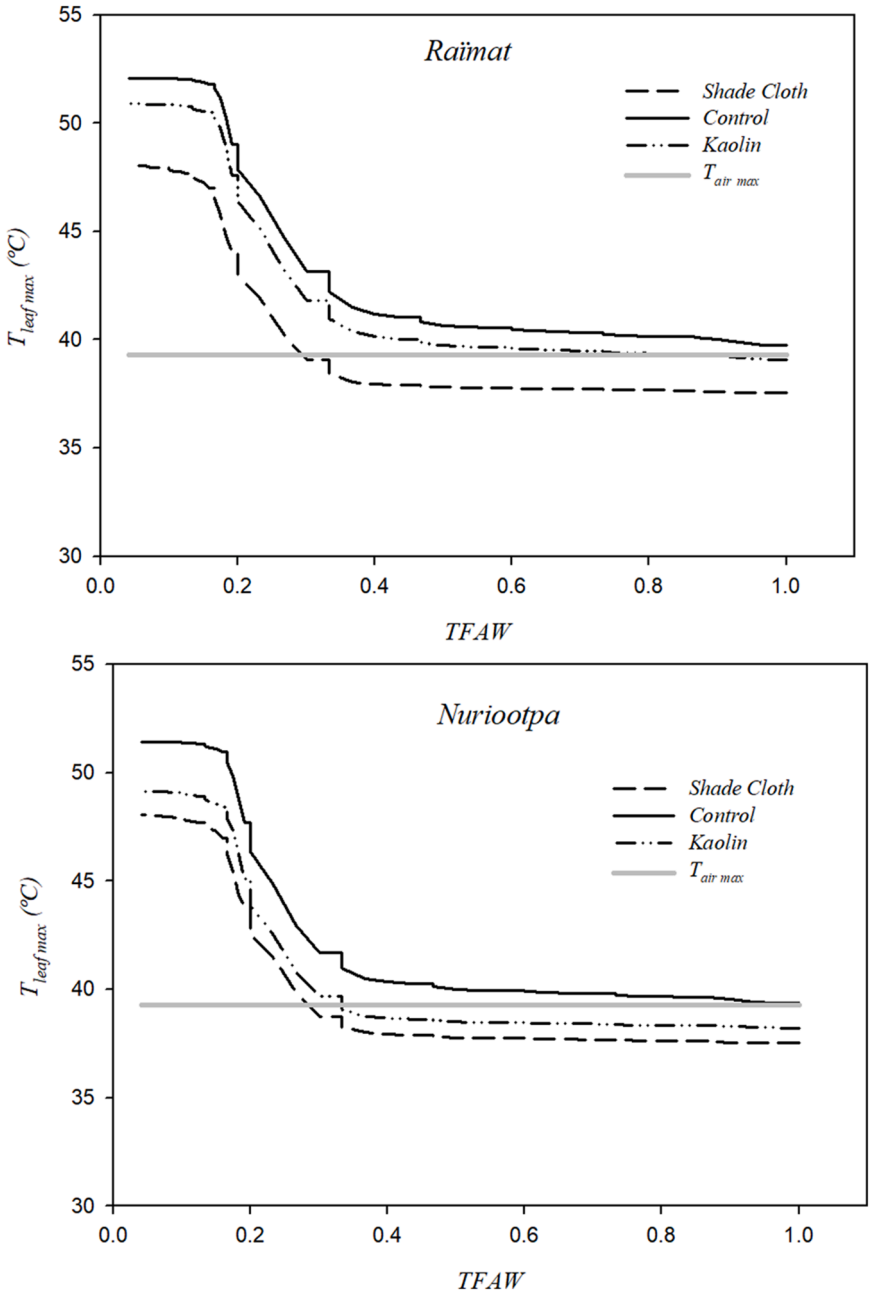

Fig. 9. Effect of the reduction on radiation load on the maximum leaf temperature ($T_{leaf\ max}$) at different soil water content levels at Raimat and Nuriootpa. Treatments are uncovered control vines (Control), vines under a 50% shade cloth (shade cloth), vines sprayed with kaolin before the heatwave (kaolin). The gray line indicates the maximum air temperature ($T_{air\ max}$) during the simulation.

light distribution associated with trellis and row orientation adds another layer of complexity to the heatwave management that needs to be further explored. The combination of varieties, orientation, and trellis could provide new avenues to improve grapevine performance in semi-arid regions.

4.4. Adaptation strategies

Current lead time for heatwave forecasting allows for vineyard irrigation before the heat event (Grace et al., 2009). However, the irrigation decision should be weighed against other factors. There are logistic restrictions related to water availability from communal systems, pump capacity on site, and price of water that limit vineyard water supply. Water allocation may be limited during dry years or at the end of the season, when heat waves are most likely but not only, reducing the viability of this practice. The efficacy of irrigation in reducing canopy temperature depends on soil moisture and the VPD during the heat wave. If TFAW is above the limiting threshold for g_s, further irrigation might be redundant.

Practices to reduce R_{int} have been proven to effectively cool the canopy. For instance, kaolin application reduced leaf temperature by 4–6 ºC in Pinot Noir (Frioni et al., 2019) and helped to maintain berry quality traits. Shellie and King (2013) found a significant increase in anthocyanin content in kaolin-treated berries when compared with untreated controls. Greer and Weedon (2013) found a reduction in berry shriveling, sunburn damage, and overripening when grapevines were protected with a shade cloth. Our results agree with these findings. Regardless of TFAW, the larger the reduction in R_{int}, the greater the cooling of the canopy (Fig. 9). However, the reduction in R_{int} involves trade-offs with reduced photosynthesis (Rosati et al., 2006; Shellie and

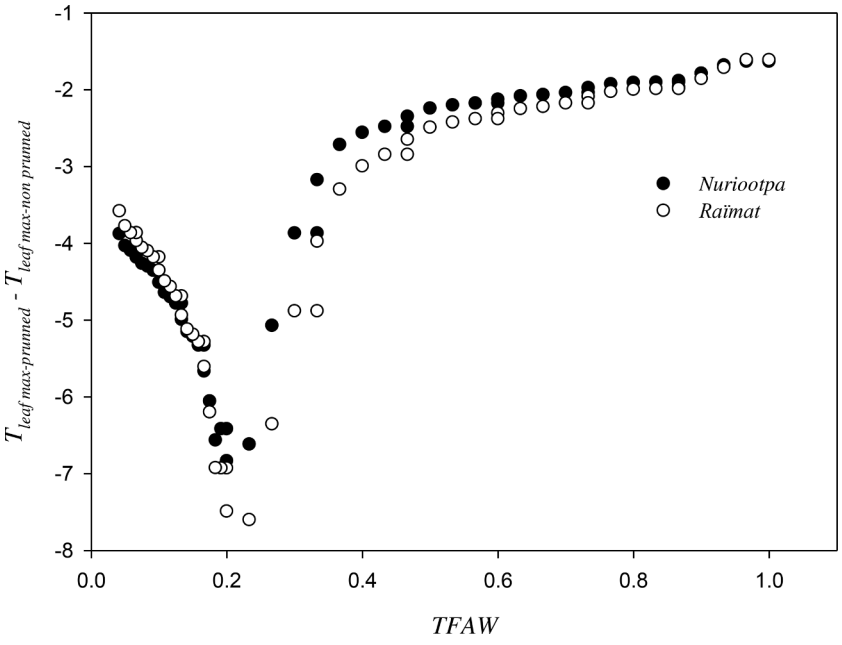

Fig. 10. The difference in sunlit leaf maximum temperature (T_{lmax}) between vines trimmed one day before a heatwave and non-trimmed controls at two locations. At Raïmat, with a VSP trellis, we assumed a topping that reduced initial canopy height 0.5 m -from 1.5 to 1 m. At Nuriootpa, with 2-wires decumbent sprawl, we simulated a lateral trimming, reducing the canopy width 0.5 m -from 1.7 m to a 1.2 m width. Each point indicates the difference in T_{lmax} between the trimmed and the control (non-trimmed) treatment.

King, 2013) and the accumulation of phenolics in the berry that may affect yield and fruit composition (Greer et al., 2011). Frioni et al. (2019) did not find photosynthesis limitation associated with kaolin application in Pinot Noir. Possibly, photosynthesis limitation is associated with the concentration used. Frioni et al. (2019) used a single application of 30 g L^{-1} whilst Shellie and King (2013) applied 60 g L^{-1} several times throughout the season. Under some conditions, canopy cooling could counteract the effect of reduced radiation on photosynthesis as found in experiments using shade cloth (Caravia et al., 2016).

Trimming to reduce heatwave damage is a less explored viticultural practice. Canopy trimming, however, is common to improve microclimatic condition and to improve berry quality traits (Herrera et al., 2015; Poni et al., 2018). It may be repeated several times during the same growing season depending on the vigor and disease pressure. In our analysis, trimming before a heatwave event was applied to modify canopy geometry and to reduce intercepted radiation. We found that trimming had a significant impact reducing canopy temperature during the heatwave. Trimming not only decreased canopy temperature by a reduction on R_{int}, but also improved plant water status and, therefore, g_s (García-Tejera et al., 2021; Li et al., 2003). The root-to-leaf area ratio modulates the plant's hydraulic resistance and the relation between plant transpiration and water potential (García-Tejera et al., 2021). Trimming increased the root-to-leaf area ratio, resulting in a more favorable supply of water for the remaining leaves (García-Tejera et al., 2021). Our model does not account for the effect of source : sink ratio on g_s and water potential (Sadras and Trentacoste, 2011; Trentacoste et al., 2011). However, the high VPD during a heatwave will limit g_s (Levin et al., 2019; Prieto et al., 2010; Soar et al., 2006); and may dampen the potential effect of source : sink ratio.

While effective in reducing canopy temperature, the scope for trimming can be constrained where availability of resources already limits canopy size. Timing and severity of the trimming need consideration. When the canopy is growing actively, a reduction in leaf area may be compensated by further growth at the expense of reserves. Trimming during ripening, after canopy has stopped growing, may increase bunch exposure and the associated risk of bunch sunburn (Gambetta et al., 2021), depending on trellising system and the row orientation. In a single-wire trellis system, lateral trimming is more likely to increase bunch exposure and temperature (Smart and Sinclair, 1976).

We did not explore the interaction between individual practices and row orientation; the implicit assumption that needs experimental testing is that these effects are additive for canopy temperature. Consistently on both sites, the NS orientation resulted in the hottest canopy (Fig. 7A and B) when maximum R_{int} during the day coincides with maximum air temperature and lowest g_s. The NW-SE orientation at Nuriootpa and the NE-SW orientation at Raïmat reduced canopy temperature by approx. 1.6 to 1.8 ºC compared to the NS orientation. These differences between NE-SW and NW-SE were an effect of the latitude and relate to the time of the day at which each orientation receives maximum R_{int} (Hunter et al., 2016). In the Northern hemisphere (Raïmat) the sun peaks in the southern half of the sky, and the NE-SW orientation has the maximum R_{int} during the morning (Fig. 8D), coincidently with the time of the day when the temperature of the air and VPD are low, and g_s peaks. Similarly in the Southern hemisphere (Nuriootpa), the sun peaks in the northern half of the sky, and the NW-SE orientation intercepts relatively more R_{int} in the morning but the less in the afternoon (Fig. 8C). We did not quantify other trade-offs between row orientation with irrigation requirements but propose that in a context of more frequent heatwaves and water scarcity, row orientation of new plantations cannot be overlooked.

We have not considered the possible cooling effect of soil evaporation on the vine microenvironment. However, this effect is likely negligible in the vineyards where drip irrigation is widespread. The wetted area underneath the canopy is unlikely to surpass 20% of the ground surface. Evaporation from a wet-bulb is a function of the radiation transmitted to the soil plus and advection effect (Bonachela et al., 1999, 2001). We do not expect that a small wet area under dripper, receiving less than 40% of the incoming radiation on average will produce a significant evaporative cooling effect. Especially for a single wire training system whose canopy completely shadows the soil area under the dripper.

5. Conclusions

Heatwave damage in grapevines depends not only on the air temperature but on other weather, soil, plant and agronomic factors, and their interactions. We showed that trellis system, row orientation, soil water availability, and weather factors including VPD, and wind speed modulate vine transpiration, water status and canopy temperature in response to heatwaves. Irrigation is a widely recommended practice and could be refined by consideration of soil water content required to maintain stomatal conductance, transpiration and evaporative cooling.

The reduction of radiation intercepted by the canopies with kaolin and shade cloth can be useful, especially when water allocation is limited. Trimming could reduce energy load and improve plant water status but may risk bunch exposure to solar radiation. Canopy trimming may be a one-off practice to implement while the canopy is still actively growing and water for irrigation can be secured to sustain further growth. The choice of a particular practice, or combination, will depend on the cost-benefit ratio to limit heatwave damage, including specific account of trade-offs.

Declaration of Competing Interest

The authors declare that they have no known competing financial interests or personal relationships that could have appeared to influence the work reported in this paper.

Data availability

Data will be made available on request.

Acknowledgments

We thank the José Castillejo Program from the Spanish Ministry of Science and Innovation for providing the fundings to Omar Garcia-Tejera to stay as a visitor scientist in the South Australian Research & Development Institute (SARDI) and PRIMA ALTOS project (No. PCI2019–103649) of the Ministry of Science, Innovation of the Spanish government.

References

AEMET, 2018. Diccionario ilustrado de meteorología. Ola de calor. Agencia Estatal de Meteorol (AEMET). https://meteoglosario.aemet.es/es/termino/169_ola-de-calor.
Allen, R.G., Pereira, L.S., Raes, D., Smith, M., 1998. Crop evapotranspiration: Guidelines for Computing Crop Water requirements. Food and Agriculture Organization of the United Nations, Rome. FAO Irrigation and Drainage Paper.
Bellvert, J., Marsal, J., Girona, J., Zarco-Tejada, P.J., 2015. Seasonal evolution of crop water stress index in grapevine varieties determined with high-resolution remote sensing thermal imagery. Irrigation Sci. 33 (2), 81–93.
Bernacchi, C.J., Singsaas, E.L., Pimentel, C., Portis Jr, A.R., Long, S.P., 2001. Improved temperature response functions for models of Rubisco-limited photosynthesis. Plant Cell Environ. 24 (2), 253–259.
Bita, C.E., Gerats, T., 2013. Plant tolerance to high temperature in a changing environment: scientific fundamentals and production of heat stress-tolerant crops. Front. Plant Sci. 4.
BoM, 2016. Climate statistics for Australian locations. Bureau Meteorol. http://www.bom.gov.au/climate/averages/tables/cw_023373.shtml.
Bonachela, S., Orgaz, F., Villalobos, F., Fereres, E., 1999. Measurement and simulation of evaporation from soil in olive orchards. Irrigation Sci. 18.
Bonachela, S., Orgaz, F., Villalobos, F.J., Fereres, E., 2001. Soil evaporation from drip-irrigated olive orchards. Irrigation Sci. 20 (2), 65–71.
Bonada, M., Buesa, I., Martin, A.M., Sadras, V., 2018. Interactive effects of warming and water deficit on Shiraz vine transpiration in the Barossa Valley, Australia. Open one. Vine Wine 52, 135–148.
Bristow, K.L., Campbell, G.S., Calissendorff, C., 1984. The effects of texture on the resistance to water-movement within the rhizosphere. Soil Sci. Soc. Am. J. 48 (2), 266–270.
Buckley, T.N., Martorell, S., Diaz-Espejo, A., Tomas, M., Medrano, H., 2014. Is stomatal conductance optimized over both time and space in plant crowns? A field test in grapevine (Vitis vinifera). Plant Cell Environ. 37 (12), 2707–2721.
Buesa, I., Mirás-Avalos, J.M., Intrigliolo, D.S., 2020. Row orientation effects on potted-vines performance and water-use efficiency. Agric. For. Meteorol. 294, 108148.
Caldeira, C.F., Jeanguenin, L., Chaumont, F., Tardieu, F., 2014. Circadian rhythms of hydraulic conductance and growth are enhanced by drought and improve plant performance. Nat. Commun. 5.
Campbell, G.S., Norman, J.M., 1998. Introduction to Environmental Biophysics. Springer, New York, xxi, 286 pages pp.
Campbell, G.S., 1985. Soil Physics With BASIC : Transport Models For Soil-Plant Systems. Elsevier, Amsterdam; New York.
Caravia, L., Collins, C., Petrie, P.R., Tyerman, S.D., 2016. Application of shade treatments during Shiraz berry ripening to reduce the impact of high temperature. Aust. J. Grape Wine Res. 22 (3), 422–437.
Caravia, L., Pagay, V., Collins, C., Tyerman, S.D., 2017. Application of sprinkler cooling within the bunch zone during ripening of Cabernet Sauvignon berries to reduce the impact of high temperature. Aust. J. Grape Wine Res. 23 (1), 48–57.
Carvalho, L.C., Coito, J.L., Colaço, S., Sangiogo, M., Amâncio, S., 2015. Heat stress in grapevine: the pros and cons of acclimation. Plant Cell Environ. 38 (4), 777–789.
Choat, B., et al., 2010. Measurement of vulnerability to water stress-induced cavitation in grapevine: a comparison of four techniques applied to a long-vesseled species. Plant, Cell Environ. no-no.
Coniberti, A., et al., 2013. Kaolin over sun-exposed fruit affects berry temperature, must composition and wine sensory attributes of Sauvignon Blanc. Eur. J. Agronomy 50, 75–81.
Corelli-Grappadelli, L., Magnanini, E., 1993. A whole-tree system for gas-exchange studies. HortScience 28 (1), 41–45.
Damour, G., Simonneau, T., Cochard, H., Urban, L., 2010. An overview of models of stomatal conductance at the leaf level. Plant Cell Environ. 33 (9), 1419–1438.
dePury, D.G.G., Farquhar, G.D., 1997. Simple scaling of photosynthesis from leaves to canopies without the errors of big-leaf models. Plant Cell Environ. 20 (5), 537–557.
DeWitt, T.J. and Scheiner, S.M., 2004. Phenotypic Plasticity: Functional and Conceptual Approaches. Oxford University Press, 198 Madison Avenue, New York, 247 pp. Dewitt, T. and Scheiner, S.
di Castri, F., Mooney, H.A., 1973. Mediterranean Type Ecosystems. Ecological Studies. Springer, Berlin, Heidelberg.
Duursma, R.A., et al., 2019. On the minimum leaf conductance: its role in models of plant water use, and ecological and environmental controls. New Phytol. 221 (2), 693–705.
Fereres, E., Orgaz, F., Gonzalez-Dugo, V., Testi, L., Villalobos, F.J., 2014. Balancing crop yield and water productivity tradeoffs in herbaceous and woody crops. Funct. Plant Biol. 41 (10–11), 1009–1018.
Frioni, T., et al., 2019. Kaolin treatments on Pinot noir grapevines for the control of heat stress damages. BIO Web Conf. 13, 04004.
Galat Giorgi, E., Sadras, V.O., Keller, M., Perez Peña, J., 2019. Interactive effects of high temperature and water deficit on Malbec grapevines. Aust. J. Grape Wine Res. 25 (3), 345–356.
Galat Giorgi, E., Keller, M., Sadras, V., Roig, F.A., Perez Peña, J., 2020. High temperature during the budswell phase of grapevines increases shoot water transport capacity. Agric. For. Meteorol. 295, 108173.
Gambetta, G.A., et al., 2012. The relationship between root hydraulics and scion vigour across Vitis rootstocks: what role do root aquaporins play? J. Exp. Bot. 63 (18), 6445–6455.
Gambetta, J.M., Holzapfel, B.P., Stoll, M., Friedel, M., 2021. Sunburn in grapes: a review. Front. Plant Sci. 11, 2123.
García-Tejera, O., López-Bernal, Á., Orgaz, F., Testi, L., Villalobos, F.J., 2021. The pitfalls of water potential for irrigation scheduling. Agric. Water Manag. 243, 106522.
Garcia-Tejera, O., Lopez-Bernal, A., Orgaz, F., Testi, L., Villalobos, F.J., 2017a. Analysing the combined effect of wetted area and irrigation volume on olive tree transpiration using a SPAC model with a multi-compartment soil solution. Irrigation Sci. 35 (5), 409–423.
Garcia-Tejera, O., Lopez-Bernal, A., Testi, L., Villalobos, F.J., 2017b. A soil-plant-atmosphere continuum (SPAC) model for simulating tree transpiration with a soil multi-compartment solution. Plant Soil 412 (1–2), 215–233.
Gonzalez-Dugo, V., et al., 2020. Empirical validation of the relationship between the crop water stress index and relative transpiration in almond trees. Agric. For. Meteorol., 108128, 292-293.
Grace, W., Sadras, V., Hayman, P., 2009. Modelling heatwaves in viticultural regions of southeastern Australia. Aust. Meteorol. Oceanogr. J. 58, 249–262.
Green, S., Clothier, B., Jardine, B., 2003. Theory and practical application of heat pulse to measure sap flow. Agron J. 95 (6).
Greer, D., Weedon, M.M., 2013. The impact of high temperatures on Vitis vinifera cv. Semillon grapevine performance and berry ripening. Front. Plant Sci. 4 (491).
Greer, D.H., Weedon, M.M., Weston, C., 2011. Reductions in Biomass accumulation, Photosynthesis in Situ and Net Carbon Balance Are the Costs of Protecting Vitis vinifera 'Semillon' Grapevines from Heat Stress with Shade Covering. AoB PLANTS, 2011.
Harris, D., Matthews, R.B., Rao, R.C.N., Williams, J.H., 1988. The physiological-basis for yield differences between 4 genotypes of groundnut (Arachis hypogaea) in response to drought 3. Dev. Processes. Exp. Agric. 24 (2), 215–226.
Hayman, P., Longbottom, M., McCarthy, M., Thomas, D., 2012. Managing vines during heatwaves [Fact sheet]. Wine Australia, Australia.
Herrera, J.C., et al., 2015. Effect of water deficit and severe shoot trimming on the composition of Vitis viniferaL. Merlot grapes and wines. Aust. J. Grape Wine Res. 21 (2), 254–265.
Hulme, M., 2020. Climates Multiple: Three Baselines, Two Tolerances, One Normal. Academia Letters.
Hunter, J.J., Volschenk, C., Zorer, R., 2016. Vineyard row orientation of Vitis vinifera L. cv. Shiraz/101-14 Mgt: climatic profiles and vine physiological status. Agric. For. Meteorol. 228–229, 104-119.
IPCC, 2014. Climate Change 2014: Synthesis Report. Contribution of Working Groups I, II and III to the Fifth Assessment Report of the Intergovernmental Panel on Climate Change [Core Writing Team R.K Pachauri and L.A. Meyers (eds)]. IPCC, Geneva, Switzerland, pp. 151–pp.
IPCC, 2018: Summary for Policymakers. In: Global Warming of 1.5°C. An IPCC Special Report on the impacts of global warming of 1.5°Cabove pre-industrial levels and related global greenhouse gas emission pathways, in the context of strengthening the global responseto the threat of climate change, sustainable development, and efforts to eradicate poverty [Masson-Delmotte, V., P. Zhai, H.-O. Pörtner,D. Roberts, J. Skea, P.R. Shukla, A. Pirani, W. Moufouma-Okia, C. Péan, R. Pidcock, S. Connors, J. B.R. Matthews, Y. Chen, X. Zhou, M.I. Gomis,E. Lonnoy, T. Maycock, M. Tignor, and T. Waterfield (eds.)]. World Meteorological Organization, Geneva, Switzerland, 32 pp.

Jackson, R.D., Idso, S.B., Reginato, R.J., Pinter Jr., P.J., 1981. Canopy temperature as a crop water stress indicator. Water Resour. Res. 17 (4), 1133–1138.
Jones, H.G., 2013. Plants and Microclimate: A Quantitative Approach to Environmental Plant Physiology. Cambridge University Press, Cambridge.
Kattge, J., Knorr, W., Raddatz, T., Wirth, C., 2009. Quantifying photosynthetic capacity and its relationship to leaf nitrogen content for global-scale terrestrial biosphere models. Glob. Change Biol. 15 (4), 976–991.
Knowling, M.J., et al., 2021. Bridging the gap between data and decisions: a review of process-based models for viticulture. Agric. Syst. 193, 103209.
Kostaki, K.I., et al., 2020. Guard cells integrate light and temperature signals to control stomatal aperture. Plant Physiol. pp.01528.2019.
Kottek, M., Grieser, J., Beck, C., Rudolf, B., Rubel, F., 2006. World map of the köppen-geiger climate classification updated. Meteorol. Z. 15, 259–263.
López-Bernal, Á., Alcántara, E., Testi, L., Villalobos, F.J., 2010. Spatial sap flow and xylem anatomical characteristics in olive trees under different irrigation regimes. Tree Physiol. 30 (12), 1536–1544.
Levin, A.D., Williams, L.E., Matthews, M.A., 2019. A continuum of stomatal responses to water deficits among 17 wine grape cultivars (Vitis vinifera). Funct. Plant Biol.: FPB 47 (1), 11–25.
Li, K.T., Lakso, A.N., Piccioni, R., Robinson, T., 2003. Summer pruning reduces whole-canopy carbon fixation and transpiration in apple trees. J. Hortic. Sci. Biotechnol. 78 (6), 749–754.
Liu, G.T., et al., 2014. Differential proteomic analysis of grapevine leaves by iTRAQ reveals responses to heat stress and subsequent recovery. BMC Plant Biol. 14 (1), 110.
Lu, Z., Radin, J.W., Turcotte, E.L., Percy, R., Zeiger, E., 1994. High yields in advanced lines of Pima cotton are associated with higher stomatal conductance, reduced leaf area and lower leaf temperature. Physiol. Plant 92 (2), 266–272.
Monteith, J.L., Unsworth, M.H., 2013. Principles of environmental physics. J.L. Monteith and M.H. Unsworth (Editors). Principles of Environmental Physics, 4th ed. Academic Press, Boston. , pp. i.
Moran, M.A., Sadras, V.O., Petrie, P.R., 2017. Late pruning and carry-over effects on phenology, yield components and berry traits in Shiraz. Aust. J. Grape Wine Res. 23 (3), 390–398.
Nairn, J., Fawcett, R., 2013. Defining heatwaves: heatwave defined as a heatimpact event servicing all community and business sectors in Australia. Centre Aust. Weather Clim. Res.
NOAA, 2020. January 202 was Earth's hottest January on Record. National Oceanic and Atmospheric Administration. https://www.noaa.gov/news/january-2020-was-earth-s-hottest-january-on-record.
North, G.B., Nobel, P.S., 1992. Drought-induced changes in hydraulic conductivity and structure in roots of ferocactus-acanthodes and opuntia-ficus-indica. New Phytol. 120 (1), 9–19.
North, G.B., Nobel, P.S., 1997. Root-soil contact for the desert succulent Agave deserti in wet and drying soil. New Phytol. 135 (1), 21–29.
Olivo, N., Girona, J., Marsal, J., 2008. Seasonal sensitivity of stem water potential to vapour pressure deficit in grapevine. Irrigation Sci. 27, 175–182.
Pagay, V., Collins, C., 2017. Effects of timing and intensity of elevated temperatures on reproductive development of field-grown Shiraz grapevines. OENO One 51 (4).
Parry, C.K., et al., 2019. An intercomparison of radiation partitioning models in vineyard canopies. Irrigation Sci. 37 (3), 239–252.
Petrie, P.R., Clingeleffer, P.R., 2005. Effects of temperature and light (before and after budburst) on inflorescence morphology and flower number of Chardonnay grapevines (Vitis vinifera L.). Aust. J. Grape Wine Res. 11 (1), 59–65.
Piñeiro, G., Perelman, S., Guerschman, J.P., Paruelo, J.M., 2008. How to evaluate models: observed vs. predicted or predicted vs. observed? Ecol. Modell. 216 (3), 316–322.
Poni, S., et al., 2018. Grapevine quality: a multiple choice issue. Sci. Hortic. 234, 445–462.
Prieto, J.A., Lebon, É., Ojeda, H., 2010. Stomatal behavior of different grapevine cultivars in response to soil water status and air water vapor pressure deficit. OENO One 44 (1), 9.
Reingwirtz, I., et al., 2021. inherent and stress-induced responses of fine root morphology and anatomy in commercial grapevine rootstocks with contrasting drought resistance. Plants 10 (6), 1121.
Roche, D., 2015. stomatal conductance is essential for higher yield potential of C3 crops. CRC Crit. Rev. Plant Sci. 34 (4), 429–453.
Rosati, A., Metcalf, S.G., Buchner, R.P., Fulton, A.E., Lampinen, B.D., 2006. physiological effects of kaolin applications in well-irrigated and water-stressed walnut and almond trees. Ann. Bot. 98 (1), 267–275.
RuralCat, 2020. Dades Agrometeorològiques. Departament d'Acció Climàtica Alimentació i Agenda Rural. Generalitat de Catalunya. https://ruralcat.gencat.cat/web/guest/agrometeo.estacions?p_auth=LDY8YW8P&p_p_id=AgrometeoEstacions_WAR_AgrometeoEstacions100SNAPSHOT&p_p_lifecycle=1&p_p_state=normal&p_p_mode=view&p_p_col_id=column-1&p_p_col_pos=2&p_p_col_count=3&_AgrometeoEstacions_WAR_AgrometeoEstacions100SNAPSHOT_action=goEstacion.
Sadras, V.O., Moran, M.A., 2012. Elevated temperature decouples anthocyanins and sugars in berries of Shiraz and Cabernet Franc. Aust. J. Grape Wine Res. 18 (2), 115–122.
Sadras, V., Schultz, H.R., 2013. Grapevine. R. D (Editors). In: Steduto, P, Hsiao, TC, Fereres, E (Eds.), Crop yield response to water. FAO, Irrigation and Drainage Paper, 66.
Sadras, V.O., Trentacoste, E.R., 2011. Phenotypic plasticity of stem water potential correlates with crop load in horticultural trees. Tree Physiol. 31 (5), 494–499.
Sadras, V., Montoro, A., Moran, M., Aphalo, P., 2012. Elevated temperature altered the reaction norms of stomatal conductance in field-grown grapevine. Agric. For. Meteorol. 165, 35–42.
Schultz, H.R., 2003. Differences in hydraulic architecture account for near-isohydric and anisohydric behaviour of two field-grown Vitis vinifera L. cultivars during drought. Plant Cell Environ. 26 (8), 1393–1405.
Shellie, K.C., King, B.A., 2013. Kaolin particle film and water deficit influence malbec leaf and berry temperature, pigments, and photosynthesis. Am. J. Enol. Vitic. 64 (2), 223–230.
Smart, R., Sinclair, T., 1976. Solar heating of grape berries and other sperical fruits. Agric. Meteorol. 17, 241–259.
Soar, C.J., et al., 2006. Grape vine varieties Shiraz and Grenache differ in their stomatal response to VPD: apparent links with ABA physiology and gene expression in leaf tissue. Aust. J. Grape Wine Res. 12 (1), 2–12.
Soar, C.J., Collins, M.J., Sadras, V.O., 2009. Irrigated Shiraz vines (Vitis vinifera) upregulate gas exchange and maintain berry growth in response to short spells of high maximum temperature in the field. Funct. Plant Biol. 36 (9), 801–814.
Swanson, R.H., Whitfield, D.W.A., 1981. a numerical analysis of heat pulse velocity theory and practice. J. Exp. Bot. 32 (1), 221–239.
Testi, L., Villalobos, F.J., 2009. New approach for measuring low sap velocities in trees. Agric. For. Meteorol. 149 (3–4), 730–734.
Trentacoste, E.R., Sadras, V.O., Puertas, C.M., 2011. Effects of the source:sink ratio on the phenotypic plasticity of stem water potential in olive (Olea europaea L.). J. Exp. Bot. 62 (10), 3535–3543.
Trentacoste, E.R., Connor, D.J., Gómez-del-Campo, M., 2015. Row orientation: applications to productivity and design of hedgerows in horticultural and olive orchards. Sci. Hortic. 187, 15–29.
Tuzet, A., Perrier, A., Leuning, R., 2003. A coupled model of stomatal conductance, photosynthesis and transpiration. Plant Cell Environ. 26 (7), 1097–1116.
van den Honert, T.H., 1948. Water transport in plants as a catenary process. Discuss Faraday Soc. 3 (0), 146–153.
Vandeleur, R., 2007. Grapevine Root hydrualics: The role of Aquaporines. University of Adelaide, Adelaide, 195 pp.
Villalobos, F.J., Fereres, E., 2017. Fitotecnia: Principios De Agronomía Para Una Agricultura Sostenible. Mundi-Prensa, Spain. Ed628 pp.
Wünsche, J.N., Palmer, J.W., 1997. Portable through-flow cuvette system for measuring whole-canopy gas exchange of apple trees in the field. HortScience 32 (4), 653–658.
Wahid, A., Gelani, S., Ashraf, M., Foolad, M., 2007. Heat tolerance in plants: an overview. Environ. Exp. Bot. 61 (3), 199–223.
Webb, L., et al., 2010. managing grapevines through severe heat: a survey of growers after the 2009 summer Heatwave in south-eastern Australia. J. Wine Res. 21 (2–3), 147–165.
Willmott, C.J., 1984. On the evaluation of model performance in physical geography. Editors. In: Gaile, G.L., Willmott, C.J. (Eds.), Spatial Statistics and Models. Springer Netherlands. Dordrecht, pp. 443-460.
Wilson, K.B., Baldocchi, D.D., Hanson, P.J., 2000. Spatial and seasonal variability of photosynthetic parameters and their relationship to leaf nitrogen in a deciduous forest. Tree Physiol. 20 (9), 565–578.